Vol. 41, No. 4 (2019) 573-591, DOI: 10.24874/ti.2019.41.04.10

Tribology in Industry

www.tribology.rs

RESEARCH

Effect of Sintering Temperature and Reinforcement Concentration on the Tribological Behaviors of Hybrid Aluminum Matrix Nano Composite

P.D. Srivyas[a,*], M.S. Charoo[a]

[a]*Mechanical Engineering Department, NIT Srinagar, Jammu and Kashmir, India.*

Keywords:

Friction
Wear
Matrix
Self-Lubrication

* Corresponding author:

Pranav Dev Srivyas
E-mail: devpranav.srivyas_17@nitsri.net

Received: 10 September 2019
Revised: 25 October 2019
Accepted: 16 November 2019

A B S T R A C T

The objectives of this experimentation is to scrutinize the effect of sintering temperature and GNP concentration on novel hybrid aluminium self lubricating nanocomposite. The tribological properties of Al-Si/ γ-Al2O3 (6 wt.%)/ GNP (4–5 wt.%) composite sample has been studied in this research.. Spark Plasma Sintering syntheses route was used for the fabrication of the composite samples. The samples were prepared at three sintering temperature i.e. 450 ˚C; 500 ˚C; 520 ˚C with dwell time constant 10 minutes. The experimentally investigated properties are friction, wear, density, for the hybrid composites samples. Tribological testing was done on the ball-on-disc configuration at room temperature under dry sliding conditions under variable load 10–50 N and upto sliding distance 450 meters with other parameters i.e. frequency, stroke remain constant. The results highlights that both sintering temperature and GNP concentration helps to enhance the overall properties of composite samples. For surface morphology; wear scar analysis, elemental percentage concentration characterization tools i.e. Scanning Electron Microscopy; Electron Dispersion Microscopy; Raman analysis is used.

1. INTRODUCTION

Aluminum alloys are broadly utilized in numerous modern applications attributable to their significant properties. these are good electrical thermal conductivities, high strength to weight proportion, high malleability, great usefulness, and great corrosion obstruction [1-2]. Now a days, Aluminum alloys have been utilized as a material in car assemblies and aircraft parts so as to make the moving vehicle lighter, which ultimately help in reducing fuel comsuption, but these aluminium alloy did not offer better tribological properties. Thus the requirement for composite materials has turned into a need for current innovation, due to the improved physical, mechanical and tribological properties [3-4]. Composites satisfy the requirement in many aspects. Composites are the structural materials that consists of two or more constituents with significantly different chemical or physical properties within the final structure to get the optimum desired properties. A composite is a multiphase

material that consist of matrix and reinforcement. For better composite it is important to have good boundary zone between the matrix and reinforcement (interface or between phase)[5]. Composites can be metal matrix composites, ceramic matrix composites, polymer matrix composites. Matrix is the main constituent in the composite which help to hold the reinforcement and to control the inter-laminar structure even at high operating temperature. The reinforcement material are the key elemennts in composites as it provides better level of strength and other mechanical as well as tribological properties. Metal matrix composites (MMCs)have received much attention because they consolidate good metallic properties (malleability and sturdiness), high modulus properties and more prominent have quality in shear and pressure even at high-temperature conditions. The broad utilization of MMCs in aviation, car ventures and in auxiliary applications has expanded because of the accessibility of economical reinforcements.

Graphene nano-platelets (GNP) [6-7] is a genuinely wonderful Nano carbon material that pulled in the consideration because of anticipated incredible mechanical, tribological, thermal and electrical properties and has turned into a subject of a consistently exploration intrigue everywhere throughout the world. It comprises of sp2 hybridized carbon atoms arranged in a honeycomb structure with a carbon-to-carbon between nuclear length, C–C, of 0.142 nm and two carbon particles and is invariant under a turn of 120^0 around any carbon molecule. Graphene-fortified aluminum nanocomposites have pulled enthusiasm from both research and industry in elite weight-touchy applications, because of the boundlessly extraordinary holding qualities of the Al matrix (metallic) and graphene (in-plane covalent + inter-plane Vander Waals). But graphene has propensity to agglomerate and stage separate in the metal lattice, which is adverse for the mechanical and tribological properties of the composite. The solid interplanar Vander Waals collaboration between graphene sheets in a metallic domain advances agglomeration as a different graphene stage, which is inconvenient for the MMNC properties [8]. However, difficulties to integrate have restricted the advancement in graphene-fortified metal matrix nanocomposites (MMNCs).

Different fabrications strategies [9-11] have been utilized for the synthesis of metal lattice composites. Particle distribution and porosity of the compound influence the mechanical properties just as the tribological properties of the manufactured composite. Dispersion of particles is either carried out by solid or fluid state processing. In the fluid techniques, particles are added to fluid aluminium matrix by mixing before casting; however, the subsequent dispersion is commonly inhomogeneous. The solid-state process includes powder metallurgy (P/M) process. P/M has incredible flexibility and ease of generation and considered as a decent strategy in delivering metal matrix composites. Powder metallurgy strategies (PM) which comprise of fundamental three stages (blending, compacting, and sintering) which offer homogeneous and uniform appropriation of reinforcement particles in the lattice. The powder metallurgy (P/M) strategy can be utilized in creating distinctive combinations in the strong state including aluminum compounds. This guarantees the sintering of difficult to-sinter materials with a generally lower temperature and shorter sintering time [12-14].

Various researches reported in this field are summarized below: Saboori et. al. [15] in their study reported that 30 % improvement in hardness of hot-pressed aluminum graphene composite fabricated using powder metallurgy. Bartolucci et al., [16] fabricate aluminum graphene composite utilized a blend by ball milling processing; hot iso-static squeezing (HIP) and the extrusion procedure for MMNCs. Bartolucci et al. [17] in another research demonstrated that the formation of Al_4C_3 can antagonistically influence the quality of the composite. This investigation recommended that improved comprehension of experimental parameters could empower acknowledging better mechanical properties of composite by concentrating on the dispersion of graphene with the Al matrix. Sahoo et al. [18] inspected the effect of processing time on the Al6061/Graphene composite manufactured utilizing the semi-strong handling procedure. Li et al. [19] endeavored to disentangle the combination strategy examined by Wang et al.

[20] by maintaining a strategic distance from the perplexing advance surface modification of Al flake by PVA. Making use of the electrostatic interaction among GO and Al flakes, Li et al. [21] accomplished a superior decrease of GO to graphene. The modulus and hardness of aluminum graphene composite with 0.3 wt.% diminished GO was estimated to be 18 % and 17 % higher than unreinforced Al manufactured under comparative conditions. Recent research concentrating on improving the dispersion of graphene in composite to improve the mechanical properties concentrated on different blend parameters. Biswas and Drzal [22] have built up a procedure that can deliver peeled graphite nano-platelets of 4–10 nm in thickness and 1 to 15 mm diameter. Wang et al. [23] have arranged Aluminum- Graphene Nano-sheets composite by utilizing 0.3 wt.% of Graphene Nano-sheets (GNS). The goal of this experimentation is to improve the elasticity of Al/GNP composite by utilizing a similar sum (0.3 wt.%) of GNPs by receiving a straightforward, efficient and effective technique. German, [24] in their study reported that solid-state diffusion assumes a noteworthy job in the development of inter molecule holding, in this way dispersion holding majorly affects the microstructure and mechanical properties. Shorowordi et al., [25] reported interface of Al-Al_2O_3 composites is Al_2O_3 dissolving into aluminium. Therefore, no transitional stages are normal at the interface. Park et al., [26]; Dobrzanski et al., [27] reported that extrusion can be utilized where better mechanical properties are required. Size and fortification of particles have an articulated impact on the mechanical properties of composites. Legitimate addition of fortifications to aluminum composites positively affects mechanical properties, for example, hardness and wears obstruction. Reduction in the % elongation was also reported. Michalski et al. [28] manufacture Cu– Al_2O_3 nanocomposites by SPS route. It was demonstrating that the impact of sintering on the matrix– reinforcement holding, densification, and hardness, has not yet been comprehended in detail. The primary point is to contemplate the impact of sintering environments and sintering systems on the microstructure and mechanical properties of the composite. M. Malaki et. al [29] in their review study on lightweight high strength metal matrix nanocomposite emphasis on the recent developments and achievements in fabrication of the nanocomposites with different nano particles. This study helps to understand the physics and basic mechanism behind the dispersion of nanoparticles in the matrix material. Therefore, fabrication route, its parameters and nanoadditive reinforcements; require further studies. The primary objective of the current study is to create diverse self lubricating composites utilizing the PM Non-Conventional Spark Plasma Sintering fabrication route. To report the impact of sintering temperature and reinforcement concentration on wear properties of hybrid aluminum matrix composite. The goal was stretched out to determine the major reason behind the enhancement of self-lubrication properties.

2. Material and Methods

2.1 Sample Fabrication

Al-Si Eutectic powder [Matrix Material] (Si 10.244 %, Fe<0.8%, Cu<0.3%, Zn<0.2%, Mn<0.15, Mg<0.1%, Al – Bal.) with normal molecule measure (APS) 60-70 μm; γ-Al_2O_3 [Primary Reinforcement] of size 20 nm; GNP [Secondary Reinforcement] 2-6 nm thickness used as the raw material for the composite. The theoritical density of Eutectic Al-Si alloy, γ-Al_2O_3 and GNP is 2.66 g/cm^3, 3.95 g/cm^3, 2.3 g/cm^3 respectively. The GNP reinforcement is first sonicated in ethanol in a ultrasonic probe sonicator for 2 hours, and then the primary reinforcement is added to the suspension and then again sonicated for 2 hours. Finally, the matrix material is added to the suspension and further sonication for 2 hours. After this, the suspension is then ball processed in high energy planetary ball mill (FRITSCH-GmbH, PULVERSETTE-5 CLASSIC, LINE) to create a homogeneous blend. For the milling, the powder was stacked in a silicon nitride container. Wet blending was done in an ethanol medium which is utilized as Process Controller Agent to avoid cold weld of the powder with the container walls. Silicon nitride balls of 10 mm measurement were utilized for the mixing with weight proportion of ball to powder is 10:1. Processing was performed at 240 rpm for 12 hours with an

intermittent stop of 15 minutes after regular intervals in order to keep up the processing temperature and to counteract sticking of the powder on the walls of the container. After the processing procedure the suspension was dried in a vacuum evaporator at 50 °C temperature for 3 hours pursued by heating in the vacuum oven at the consistent temperature of 50 °C for an hour in order to totally expel the dampness content. To avoid oxidation of the powder, the processed powder was kept in the glove box to limit the oxidation of the powder. Two compositions were blended i.e. Al-Si – 6 wt.% γ-Al_2O_3 – 4 wt.% GNP and Al-Si – 6 wt.% γ-Al_2O_3 – 5 wt.% GNP.

In this study a non-conventional P/M processing technique i.e. Spark Plasma Sintering (SPS) is used. The spark plasma sintering strategy is getting to be famous because of the favorable circumstances of the technique and the upgraded material properties, just as lower preparing temperature and shorter sintering time to unite powders contrasted with ordinary strategies. Sintering at lower temperatures and shorter occasions diminishes the danger of vaporization, limits grain development and renders cleaner grain limit. Spark plasma sintering (SPS) utilizes low voltage, DC current, and uniaxial strain to merge powders. Processing of the powder was done by utilizing standard graphite die on of diameter 30 mm for the creation of the sample in the SPS [Dr. Sinter-SPS-625, - Fuji-Electronic-INDUSTRIAL-C0. Ltd. JAPAN]. The manufacturing was done at 450 °C; 500 ˚C and 520 ˚C Sintering temperature for each composition samples at a heating rate of 100 °C/min; load of 50 MPa all through the entire procedure; holding time 10 minutes under argon atmosphere. The sintering is done in controlled air which empowers controlled decrease and prompts the creation of completely thick samples. This procedure does not require pre-compaction as the compaction and sintering go hand in hand. Clear grain limits; increment in versatility; improved interfacial holding; isolation of decreased debasements are key accomplishments of this manufacturing route. The entire procedure of the sample fabrication test takes 14 minutes and 30 seconds. For the composition Al-Si – 6 wt.% γ-Al_2O_3 – 4 wt.% GNP at 520 ˚C the sample fails i.e. the sample melts and evaporates which leads to failure at this temperature. The sintered samples were then expelled from the die after quick cooling procedure. The sintered examples were then cleaned by using polishing machine utilizing SiC emery paper with (220-2000) grit size. The samples were then cleaned utilizing diamond paste (5-0.25 μm) on the velvet paper to get the mirror cleaned surface.

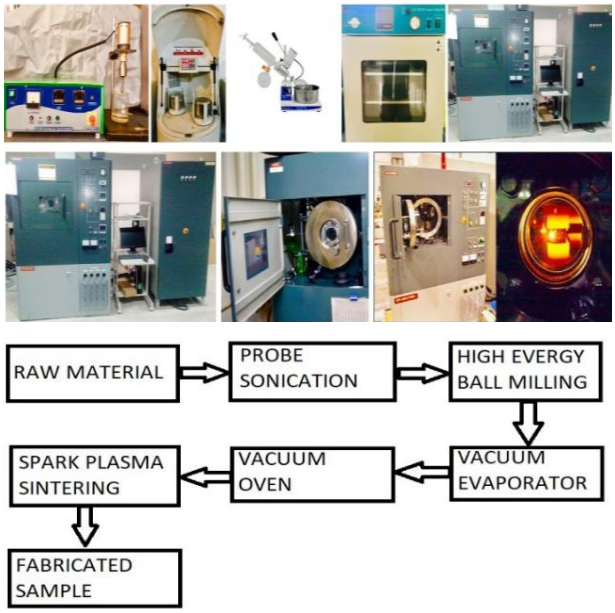

Fig. 1. Experimental procedure of sample fabrication.

2.2 Experimental Procedure and Characterization

Dry sliding experimental tribological tests were conducted on Ball-on-Disc Reciprocating Tribometer (R-Tech Universal Tribometer) in Room Temperature. The tribometer is sensor-controlled and has a proper data actuation system is used to execute the test and to save the output results. The load tribo-tests were conducted for the varying load (10N – 80N); with other parameters, stroke 2mm, frequency 30 Hz, Sliding Distance 120 meters that remain constant. The sliding distance tests were also conducted to study the behavior of sliding distance on the composite sample. The sliding distance tests were conducted in 5 steps for 450 meters i.e. , 180 meters, 270 meters, 360 meters, 450 meters with load 20N and rest the parameters remain the constant. For the tribological test, the counter-body used is the chrome steel ball plated with chromium. Before and after each test the samples are properly cleaned with the acetone in the ultrasonic bath so as to remove the impurities

from the sample surface and then drying in the vacuum oven. Various tools i.e. SEM (HITACHI S3600N), EDS (HITACHI S3600N), 3-D Surface Profilometer (R-tech Optical Microscopy (Leica DM 6000M) were used for the various pre as well as post-testing characterization.

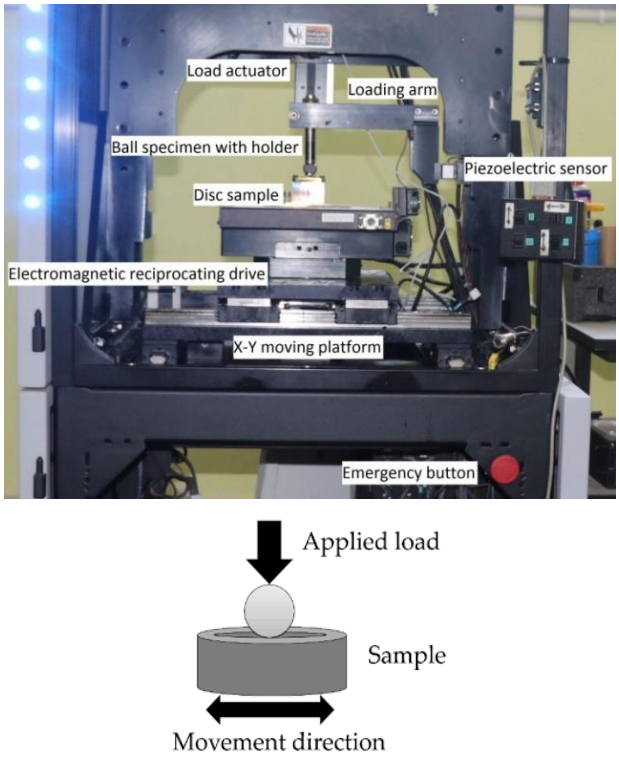

Fig. 2. Ball-On-Disc Configuration of Universal Reciprocating Tribometer and Schematic diagram.

3. Results and Discussions

3.1 Density Results

The theoretical densities and practical density of the hybrid composite samples using rule of mixture and Archimedes method. The theoritical density of Eutectic Al-Si alloy, γ-Al_2O_3 and GNP is 2.66 g/cm³, 3.95 g/cm³, 2.3 g/cm³ respectively. Equation 1 given below helps us to determine the theoretical density of the composite samples.

$$\delta_m = \frac{W_{al}+W_{alu}+W_{gnp}}{\frac{W_{al}}{\rho_{al}}+\frac{W_{alu}}{\rho_{alu}}+\frac{W_{gnp}}{\rho_{gnp}}} \quad (1)$$

δ_m Theoretical density of the mixture.

W_{al} Weight percentage of aluminum alloy powder.

W_{alu} Weight percentage of nano-alumina powder.

W_{gnp} Weight percentage of graphene nano platelets.

ρ_{al} Specific weight of the base aluminum alloy.

ρ_{alu} Specific weight of nano-alumina powder.

P_{gnp} Specific weight of graphene nano platelets.

Based on (1), the theoretical density values and the practical values of the reinforced composites are calculated (table 1). The bulk density/Practical density (ρ_p) of the sintered sample was measured using digital Densimeter based on Archimedes principle. Highly dense and compact samples were obtained using the SPS fabrication route at low temperature.

$$\rho_p = \frac{W_{air}}{W_{air}-W_{water}} \quad (2)$$

ρ_p Bulk density / practical density after sintering.

W_{air} Weight of the sample in air.

W_{ater} Weight of the sample in water.

Porosity volume percentage of the sintered sample was calculated according to equation 3 given below.

$$\text{Porosity (\%)} = 100 - \frac{\textit{Sintered Density}}{\textit{Theoritical Density}} \times 100 \quad (3)$$

Table 1. Theoritical Density, Measured Density & Porosity content of composite sample w.r.t sintering temperature and composition.

Composition / Sintering Temp.	Theoretical Density (g/cm³)	Measured Density (g/cm³)	Relative Density (%)	Porosity content (vol.%)
Hybrid Composition 5 (HC5-450) / 450 °C / Al-Si +6 wt.% Al_2O_3 + 4 wt.% GNP	2.727	2.5229	92.51	7.48
Hybrid Composition 5 (HC5-500) / 500 °C / Al-Si +6 wt.% Al_2O_3 + 4 wt.% GNP	2.727	2.6698	97.90	2.097
Hybrid Composition 6 (HC6-450) / 450 °C / Al-Si +6 wt.% Al_2O_3 + 5 wt.% GNP	2.724	2.4972	91.57	8.325
Hybrid Composition 6 (HC6-500) / 500 °C / Al-Si +6 wt.% Al_2O_3 + 5 wt.% GNP	2.724	2.6631	97.76	2.235
Hybrid Composition 6 (HC6-520) / 520 °C / Al-Si +6 wt.% Al_2O_3 + 5 wt.% GNP	2.724	2.6913	98.79	1.200

From the density, porosity content measured results, it is revealed that the increase in the temperature leads to increase in the relative density and reduces the porosity content in the fabricated composite [35-36]. With the increase in the relative density the micro hardness of the sample also increases. The hardness value is attributed to higher density value. Similar studies were reported [30–34]. It was reported that increase in the sintering temperature reduces the amount of large pores and also reduce grain size indeed increases density. They attributed decrease in the porosity to the increases hardness. In this particular research two compositions samples are fabricated at diffrerent sintering temperature and it is observed that with higher sintering temperature of 520 °C higher relative density 98.79 % is achieved for HC6 composition, which is comparatively high for the same composition sample fabricated at 450 °C and 500 °C. Hence this study conforms that the sintering temperature has an impact on the density and porosity vol. content of the fabricated samples. It is also observed that the density of the composite sample decreases with the amount of the GNP increases. This decrease was not so significant as there is minute difference in the density of the both compositions atsimilar sintering temperature. This minute decrease in the density was related to the increase in the soft GNP reinforcement.

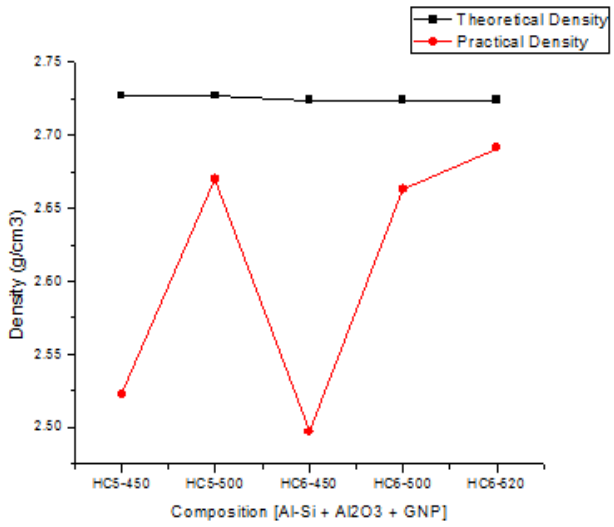

Fig. 3. Density graph with respect to reinforcement concentration & sintering temperature.

3.2 Friction and Wear studies

Dry condition tribological tests were conducted at Room temperature on ball-on-disc reciprocating universal tribometer to study friction and wear of Spark Plasma Sintered specimen against chromium plated chrome steel ball. Load test (10-80 N), as well as the sliding distance, was performed in this study. For load test; load varies from 10-80 N with other parameters i.e. sliding distance (120 meters), frequency (30 Hz); stroke (2 mm); remain constant. Sliding distance tests were conducted for 90 meters to 450 meters of sliding distance in equal five steps with other parameters i.e. load, frequency, stroke remains constant throughout. Moreover, the wear volume of the scar was calculated using Rtech 3D-Profilometer. In addition, equation 4 was used to determine the wear coefficient.

$$Wear\ Rate = \frac{Wear\ Volume}{Sliding\ Distance \times Load} \quad (4)$$

Results for COF versus load for different compositions specimens were shown in Fig. 4. COF versus sliding distance results shown in Figs. 7 and 8. Wear volume versus load for all specimens was shown in Fig. 5. Sliding distance versus Wear volume of all specimens was shown in Fig. 9. The wear coefficient versus load graph is shown in figure 6. Sliding distance versus wear coefficient for all specimens shown in Fig. 10. COF for hybrid composition 5 – 450 (HC5-450) is shown in Fig. 4. For HC5-450 the COF first increases as load increases from 10-20 N load and then decreases at 30 N load and report the lowest value for COF (0.1039). After 30 N load up to 80 N load, the value for COF almost remains constant with a very little fluctuation in the COF value. COF Maximum value was obtained at 20 N load (0.1595). Form Fig. 4, it is clear that 4 wt.% GNP reinforcement composite sample with fabricating at 500 ˚C (HC5-500) shows maximum COF value at 10 N load (0.2028) and minimum at 70 N load (0.1313). The continuous decrease in the COF was reported for this composition. Maximum (0.2405) and minimum (0.1495) COF was observed at load 10 N and 50 N respectively for HC6-450. COF continuously decreases for hybrid composition 6–450 from 10-50 N load, and then again increases, shown in Fig. 4. In hybrid composition 6-500, COF trend is first Continuous decrease up to 60 N load (0.1291) and further increase with load. The maximum COF was reported at 10 N (0.1818) shown in Fig. 4. For hybrid composition 6-520, minimum COF (0.1165) is at 10 N load and maximum (0.164) was reported at 20 N load.

Wear volume for HC5-450 increases linearly with the load. Maximum (0.0707076mm^3) and Minimum (0.0400167 mm^3) wear volume was reported at 80 N and 10 N load respectively. HC5-500 shows a similar trend as HC5-450 but comparatively less wear volume is reported. Minimum wear volume (0.0297654 mm^3) at 10 N and maximum (0.0497686 mm^3) at 80 N load was reported. The wear volume for HC6-450 increases as load increases. Wear volume minimum value (0.039764 mm^3) and maximum (0.062305 mm^3) was reported at 10 N and 80 N load respectively. HC6-500 shows a minimum wear volume of (0.0323654 mm^3) at 10 N and maximum wear volume (0.0555622 mm^3) at 80 N load. HC6-520 shows similar linearly increases trend as load increases. HC6-520 reported maximum (0.039965 mm^3) and minimum (0.019231 mm^3) wear volume at 70N and 10N load. The wear coefficient for HC5-450 gradually decreases with load increases. Wear coefficient maximum (3.33473E-05 mm^3/N.m) and minimum (7.25968E-06 mm^3/N.m) was obtained at load 10N and 70N load respectively. The wear coefficient for HC5-500 shows a decreasing trend with increasing load. The maximum wear coefficient (2.48045E-05 mm^3/N.m) for 10 N and minimum (5.18423E-06 mm^3/N.m) for 80 N was obtained. Wear coefficient for HC6-450 (1.80197E-05 mm^3/N.m) maximum and (6.49007E-06 mm^3/N.m) minimum was reported at 20N and 80 N load. The maximum wear coefficient (2.69712E-05 mm^3/N.m) at 10 N and minimum of (5.31603E-06 mm^3/N.m) at 50 N load was reported for HC6-500. Wear coefficient for HC6-520 minimum (4.15896E-06 mm^3/N.m) at 80 N and maximum (1.60256E-05 mm^3/N.m) at 10 N load was observed.

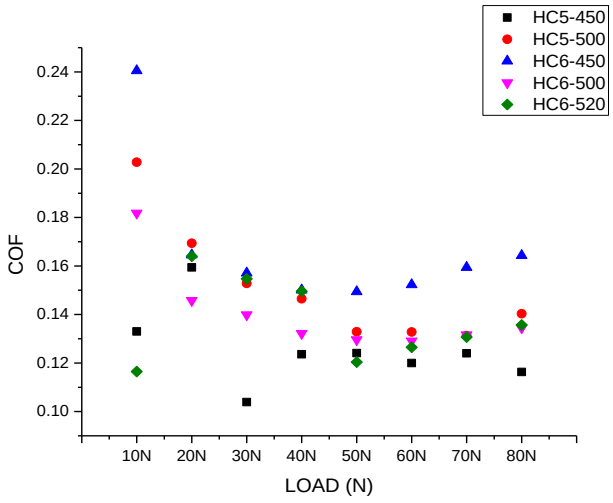

Fig. 4. Load v/s COF graph for different composite samples fabricated at variable temperatures.

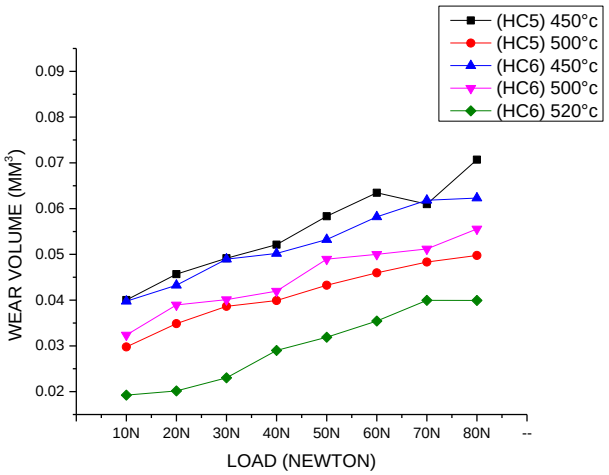

Fig. 5. Load v/s wear volume graph for samples fabricated at variable temperatures.

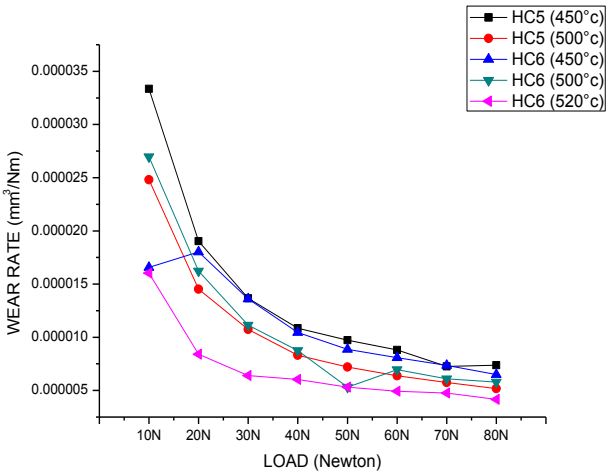

Fig. 6. Load v/s wear rate graph for samples fabricated at variable temperatures.

From the COF graph, it is observed that lower COF is in the composition sintered sample at 450 °C for HC5 Composite. But this composition sample offers max wear rate (material removal) while testing. This might be due to the low bonding of the particles of the composite sample due to the low sintering temperature. While tribo testing this composite material offeres minimum wear resistance toward the counterbody and shows minimum COF and easy removal of the material. Hence less sintering temperature leads to less dense and compact sample which offer high wear of the material due to lack of the bonding between the particles. The low wear volume of the self lubricating composite are attributed to the weak layered lamellar structure of the solid lubricant (GNP). Direct metal-metal contact on the relative motion surface produce COF and plastic deformation of the surface. GNP presence in the composite leads to the formation of the tribolayer which enhance the friction and wear mechanism.

As sliding contineous the plastic deformation layer get removed from the contacting surface which leads to asperity contact. These plastic deformed particles stick back to the counterbody leads to form a low shear stress junction of lubrication film [37]. This junction shows protective lubrication behaviour hence shows easy sliding which indeed reduce wear volume of the composite [38,39]. It was observed that the wear rate of the composite sample decreases with the increasing load. This might be due to the increasing load, due to contact pressure severity over the asperities tips [40]. This enormous applied load, increases the interface temperature and hence yield strength. Ultimately reduces the wear rate of the hybrid composite [41]. It is also observed that the higher concentration of the GNP precipitate is also responsible for the production of large protuberance on wear scar and reduce the chance for the matrix particles to come in direct contact with the counterbody hence decrease the wear rate [42].

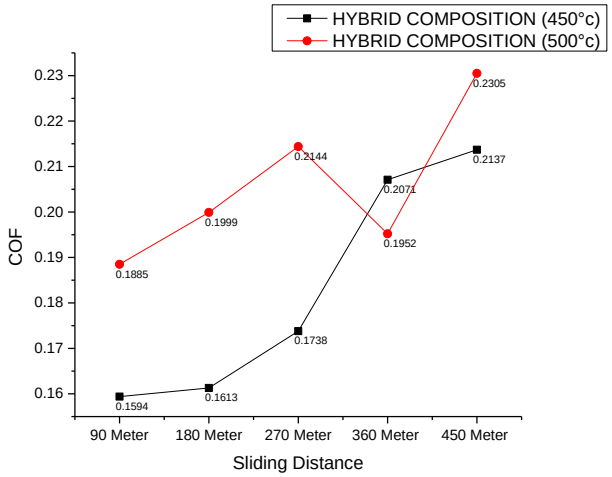

Fig. 7. Sliding Distance v/s COF (Hybrid Composition 5; Al-Si +6 wt.% Al_2O_3 + 4 wt.% GNP).

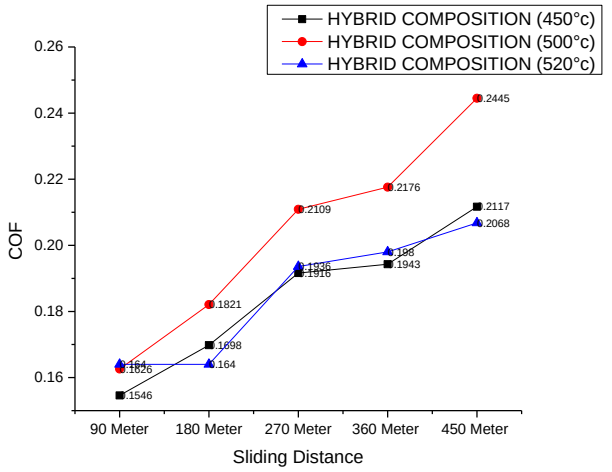

Fig. 8. Sliding Distance v/s COF (Hybrid Composition 6; Al-Si +6 wt.% Al_2O_3 + 5 wt.% GNP).

Sliding Distance versus COF for HC5-450 shown in Figs. 7 and 8. Under dry sliding conditions, COF for HC5-450 increase up to 270 meters and afterward decrease at 360 meters and again increases for 450 meters and achieve maximum value for the COF (0.2305). Minimum (0.1885) COF was observed at a sliding distance of 90 meters. COF continuously increase for HC5-500 from 90 meters to 450 meters; maximum COF (0.2137) and minimum COF (0.1594) was reported for 450 meters and 90 meters respectively, as shown in Fig. 7. A gradual increase in the COF with sliding distance was reported for HC6-450. As shown in the figure, Maximum COF (0.2117) and minimum COF (0.1546) were reported at 450 meters and 90 meters. A linear increment in the COF with increasing sliding distance for HC6-500 was observed. The minimum COF (0.1626) is at 90 meters and the maximum (0.2445) was reported at 450 meters, shown in Fig. 8. Liner increment in COF for HC6-520 was reported. Maximum (0.2068) and minimum (0.164) COF was reported at 450 meters and 90 meters respectively.

Wear volume linearly increase for HC5-450, with sliding distance. Wear volume maximum (0.380522 mm^3) and Minimum (0.049876 mm^3) value were reported at 450 meters and 90 meters respectively. For HC5-500 liner trend in wear, volume was reported. Wear volume Minimum (0.034867 mm^3) at 90 meter and maximum (0.208523 mm^3) at 450 meters was reported. HC6-450 Wear volume increases proportionally with sliding distance. The minimum value (0.038956 mm^3) and maximum (0.29762 mm^3) wear volume were observed at 90 meters and 450 meters respectively. HC6-500 shows the minimum wear volume of (0.028951 mm^3) at 90 meters and maximum wear volume (0.154074 mm^3) at 450 meters. HC6-520 shows similar linearly increases trend as previous compositions, with maximum (0.084546 mm^3) at 450 meters and minimum (0.017549 mm^3) wear volume at 90 meters. The maximum Wear coefficient for HC5-450 (4.22803E-05 mm^3/N.m) was obtained at 450-meters sliding distance and minimum (1.69941E-05mm^3/N.m) wear coefficient was obtained at 270 meters sliding distance. Wear coefficient for HC5-500 was Maximum (2.31692E-05 mm^3/N.m) and minimum (1.43519E-05 mm^3/N.m) at 450 meters & 180 meters. Wear coefficient for HC6-450 (3.30689E-05 mm^3/N.m) maximum and

(1.37371E-05 mm³/N.m) minimum was reported at 450 meter & 360 meters. Wear coefficient for HC6-500 offer minimum value (1.21788E-05 mm³/N.m) at 360 meter and maximum (1.71193E-05 mm³/N.m) at 450 meters. HC6-520 Wear coefficient minimum value (8.40706E-06 mm³/N.m) and maximum (9.74952E-06 mm³/N.m) was reported at 180 meters and 90 meters respectively.

For the sliding distance test the COF continuous increases with the increasing sliding distance for the composite samples. It is attributed to direct contact at the asperity level between the matrix and the counter body which increases traction friction as the matrix is prone to adhere to counter body. This is because of the mutual high solid solubility of the matrix and counterbody. It is well known that higher solubility leads to higher adhesion with mating surface , results higher friction [45–46]. It was observed that the graphene oxide layer exists after the initial run in period, but as the sliding continuous for the longer sliding distance these oxide layer get plastically deformed from the composite and get removed leads to have direct asperity – asperity contact which increases the COF for the sliding distance test [43]. After the initial run in period a strong mechanical mixed layer (MML) is formed between the tribopair due to the plastic deformation of the oxide layer with increasing temperature. A similar trend was observed with all the composite sample. In this case, the matrix material come in direct contact after the initial run in period as the plastic deformation removed the oxide layer. As the counterbody comes in direct contact and fractured Si precipates generate the strain with in the matrix at the mating surface. Silicon precipates support the sub-surface crack growth and delamination of the surface. Due to the delamination and removal of MML junction the sub surface asperites come in direct contact leads to increase COF and cause three-body abrasion; forms longitudinal grooves as wear scar. This leads to high wear volume and wear rate for the 450 meter sliding distance test [42]. It is also observed that the sintering temperature also effect the wear rate of the composoite. HC6 compositio fabricated at 520 °C achieved lowest volumetric loss. This is because fabrication of highly dense and compact sample which reduces the porosity content and increases the hardness hence reduce the volumetric loss. As wear resistance is directly proportional to the hardness of the material [35 – 36].

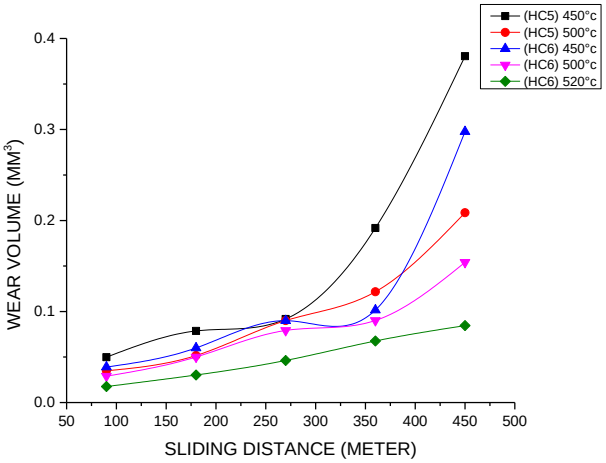

Fig. 9. Sliding Distance v/s wear volume graph for samples fabricated at variable temperatures.

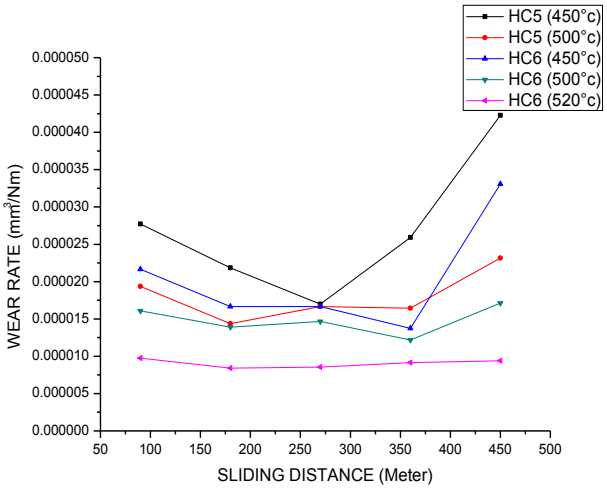

Fig. 10. Sliding Distance v/s wear rate graph for samples fabricated at variable temperatures.

3.3 Worn Surface Characterization

Wear map and different wear regimes were identified as the function of load. The basic wear modes are as follows:

a) Mild Wear: This wear mechanism is for a low load regime. In this wear oxidation layer is formed. This wear regime is also characterized by abrasion and cracking of the oxidation layer/ transfer layer/ protective film. Mild wear regime was attributed because of the stable formation of tribolayer. Transfer of material from one surface to other results in the consolidation of oxidized and plastically deformed particles into hard surface thus protect/ reduce further wear of the

material. Scoring is also a prominent wear mechanism in mild wear regime.

b) Severe Wear: In this wear regime delaminating wear was operated by deformation and cracking of subsurface. Wear mechanisms such as fretting; fatigue and adhesion are also related to severe wear. In this wear regime, normal as well as tangential load cause cyclic plastic deformation of surface. Pitting wear is also a predominant factor that causes severe wear.

c) Seizure & Scuffing Wear: in this wear regime, mating surface temperature and local weld are high which lowers the shear strength of the sub-surface layer. Under this wear regime the load is not directly proportional to the wear rate of the material. Sticking and melt wear are other main reasons for seizure and scuffing wear of material.

Resistance to the motion generates friction which further leads to wear in the material. Friction forces are experienced when the object surface is moved tangentially with respect to the counter body or when a body attempts to move from rest. The friction force is important in the fact that total energy consumption includes 45% of friction losses and further leads to wear. When one surface is in contact with another, asperity-asperity contact takes place. At high critical load and pressure, local weld and junction-junction interface shared off due to relative motion cause by adhesion wear. It was reported that in dry sliding tribo-conditions the impact of adhesive wear is twice as that of under lubrication conditions. Other wear modes are Pitting, corrosion, abrasion, plastic deformation, etc. Wear of the material changes from mild wear to severe wear within the sliding distance. In dry sliding condition wear of Al-Si alloy, it varies as the function of the applied load. It was reported that the oxidation of aluminum alloys and composite play a very important role in the formation of wear debris as well as tribolayer. Tribo-layer stability is much more at low load and helps to reduce the COF as well as wear. As the load increased the wear rate increases proportionally. At high load wear is characterized by significant transfer of material on the mating surface. Another wear mechanism i.e. delaminating layer was observed in this wear regime where tribolayer is removed and cracked by sub-surface plastic deformation. For composite the wear rate is less as compared to alloy due to the load-bearing capacity of the reinforcements. Another crucial parameter that affects wear is fracture toughness. Wherever the magnitude of the load is higher than the load-bearing capacity and fracture strength of the reinforcement another wear regime starts.

An optical micrograph of a dry sliding wear test was done to analyze the predominant wear mechanism. From the studies, it was observed that the formation of the oxide layer i.e. tribolayer takes place on the contacting surface. Adhesion; three-body abrasion, plastic deformation, delaminating and oxide wear are the prominent wear mechanism. For low load (10 and 20 N) main wear mechanism is the adhesion which was due to the broken asperities. Increases in the adhesion wear, as well as abrasion wear, was observed with increased load. Two types of lubrication phenomena take place i.e. tribolayer lubrication and broken asperities ball-bearing effect that carries the load while testing. For the sliding distance test, grooves become smoother and reveal the formation of the graphene oxide layer at the interface. Due to the tribofilm between the mating surfaces, direct contact at interface reduces and significantly reduces adhesion as well as plastic deformation of the composite sample and hence reduces the wear. At 50N load, mild adhesion, as well as smooth surface, was reported which reduce the plastic deformation of the asperities and hence reduce wear. Under the tribolayer there is shear layer where high shear gradient exists. These shear layers consist of soft as well as hardened layers. The soft layer consists of the crack void and the hard layered is because of plastic deformation which leads to the work hardening of the tribo layer.

Hybrid composition 5 (450 ˚C) (Sliding Distance)

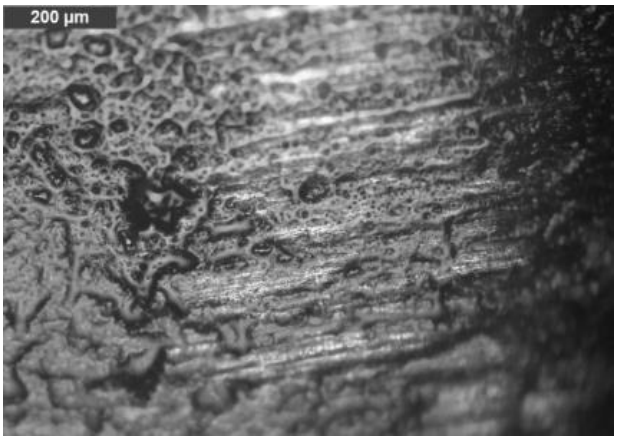

Hybrid composition 5 (500 ˚C) (Sliding Distance)

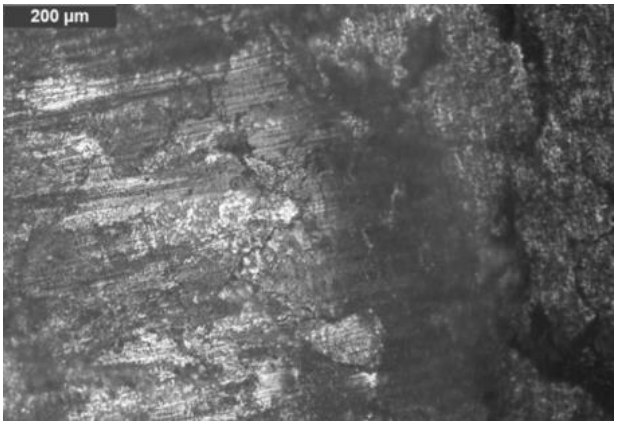

Hybrid composition 6 (450 ˚C) (Sliding Distance)

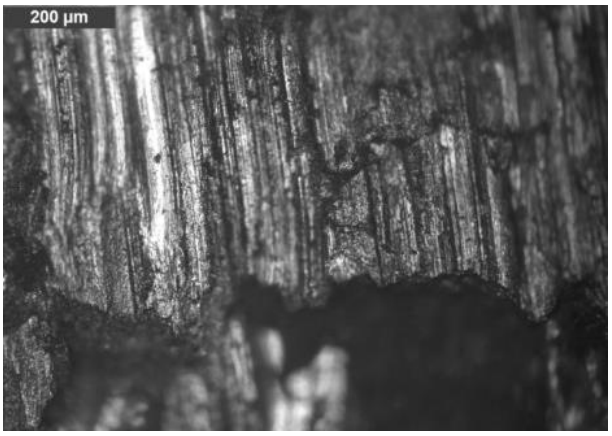

Hybrid composition 6 (500 ˚C) (Sliding Distance)

Hybrid composition 6 (520˚C) (Sliding Distance)

Counter Body (Wear scar)

Fig. 11. Optical micrographs of wear scar on different composite samples.

SEM analysis was performed on the wear scar of hybrid composition to analyze the wear mechanism. It was observed that tribolayer is formed on the wear scar surface hence reduce COF and wear volume. The presence of tribolayer reduces direct metal-metal contact between the sliding contact surface reduces the adhesion. Mild adhesion was also observed in the SEM images which are due to the transfer of the material. EDS analysis confirms the formation of the tribolayer and adhesion wear of the material. Plastic deformation was also observed on the sample scar which is because of the rise in the temperature in dry conditions. An increase in the temperature leads to the softening of the material at the interface that leads to higher plastic deformation. It is noticeable that prominent wear mechanism was mild adhesion; tribolayer formation and plastic deformation. The surface also include abrasion, severe plastic deformation, deep scuffing as well as metallic wear at some surface for higher sliding distance and even at higher load. But most often the rubbed surface shows smooth surface. Some obious scratches

are formed which signify high wear for the sliding distance test scars. The worm surface for the self lubricated surface shows more dense wear scar and grooves which dominate abrasiove wear [43 – 44]. By the introduction of the GNP in most test case the tribo oxide layer formed which prevents the rubbing surface from the direct contact significantly enhance the tribololgical properties [42].

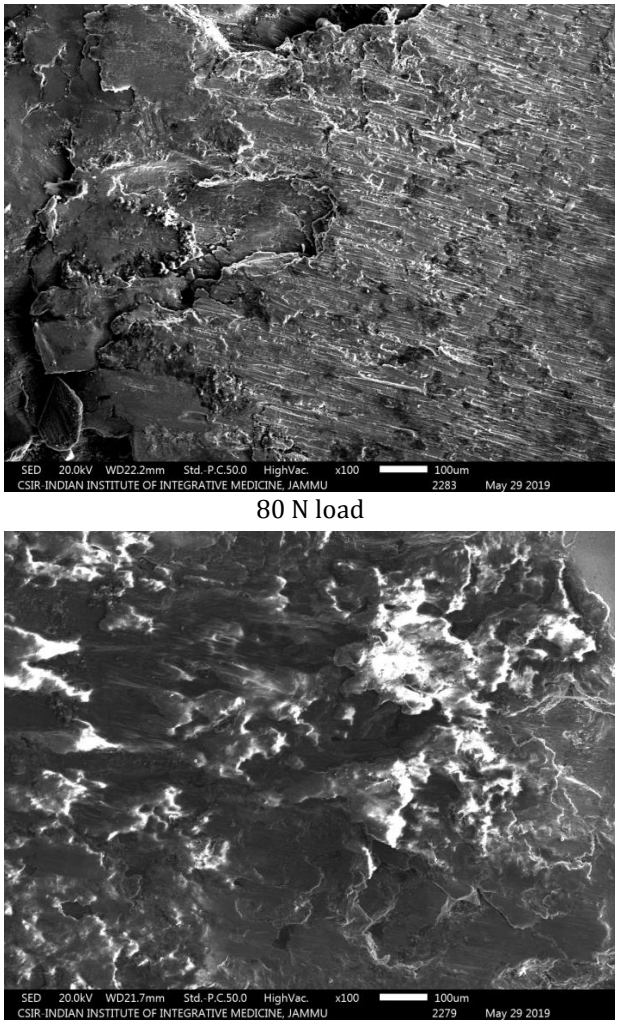

Fig. 12. SEM micrographs of Hybrid composition-5 (500 ˚C) wear scar (80 N; Sliding Distance 450 m).

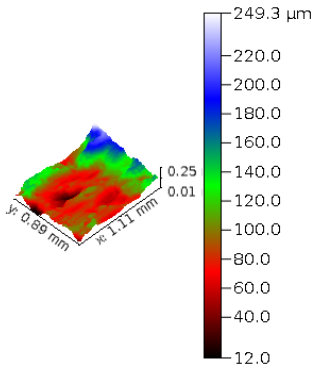

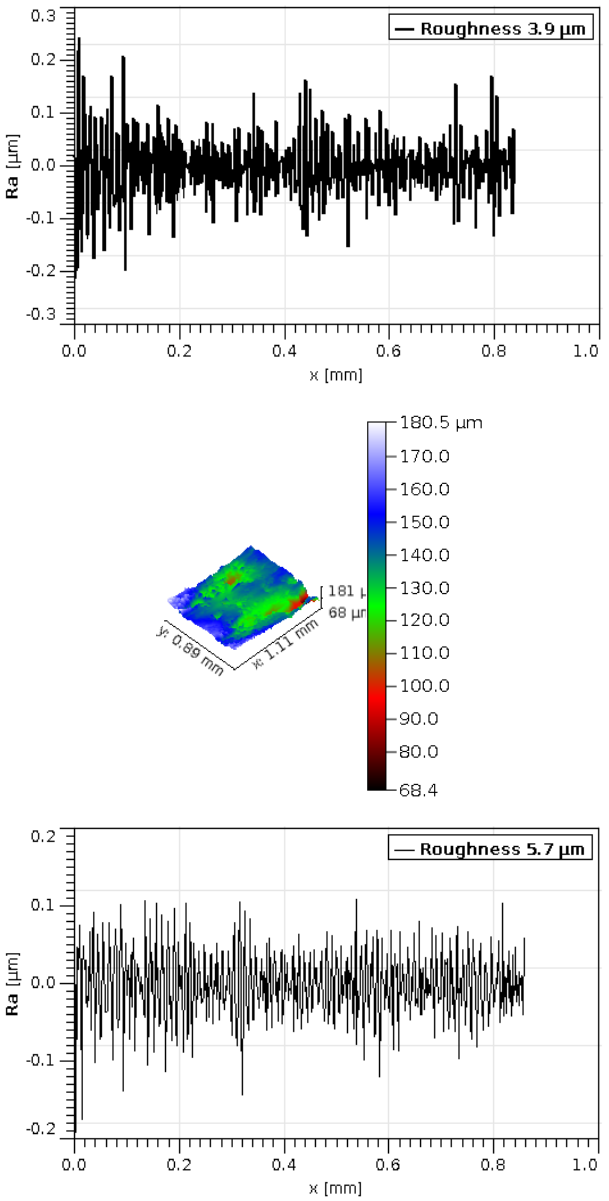

Fig. 13. 3-D Surface Profilometer micrographs of wear scar on Hybrid composition 5 (450 ˚C) (80 N; Sliding Distance 450 m).

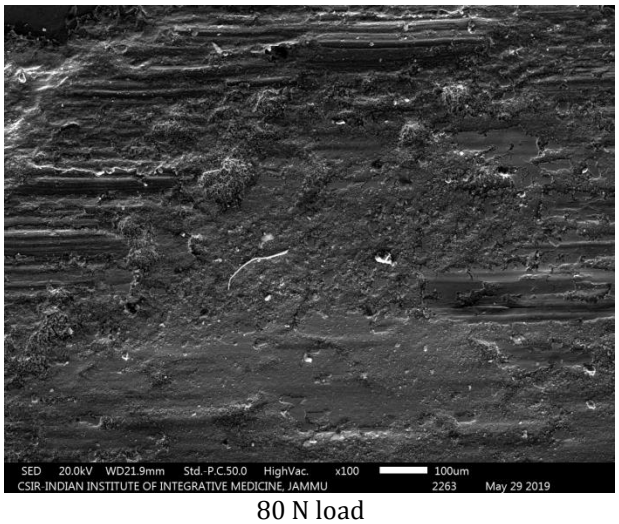

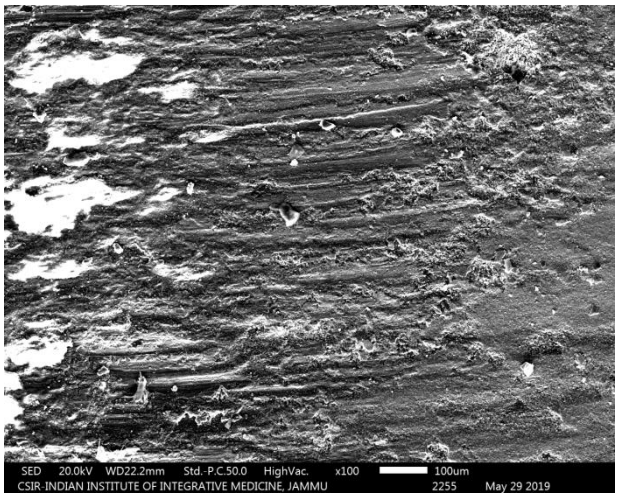

Sliding Distance (450 meters)

Fig. 14. SEM micrographs of Hybrid composition-5 (500 ˚C) wear scar (80 N; Sliding Distance).

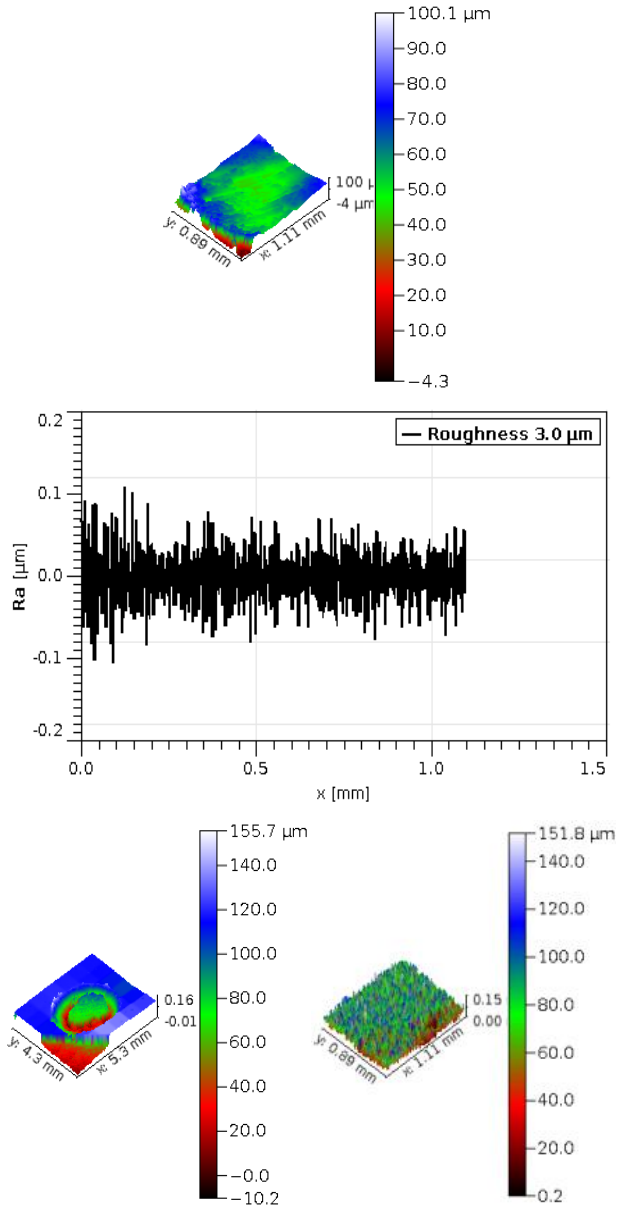

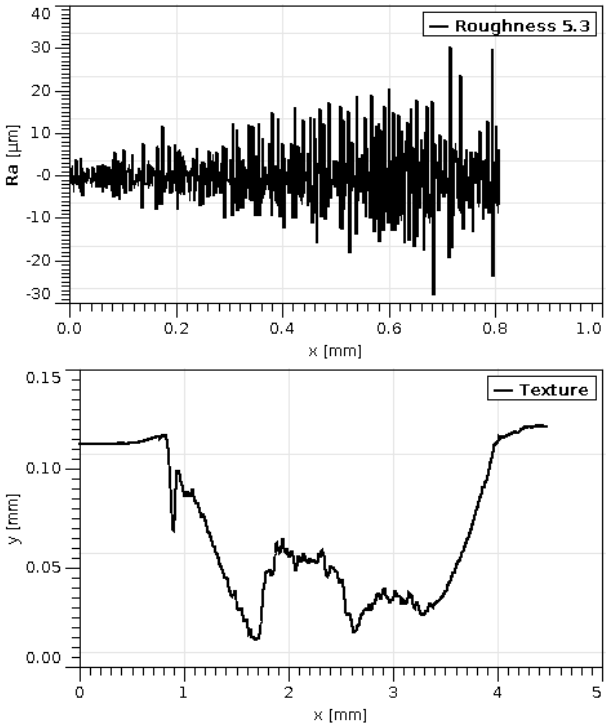

Fig. 15. 3-D Surface Profilometer micrographs of wear scar on Hybrid composition 5 (500 ˚C) (80 N; Sliding Distance 450 m).

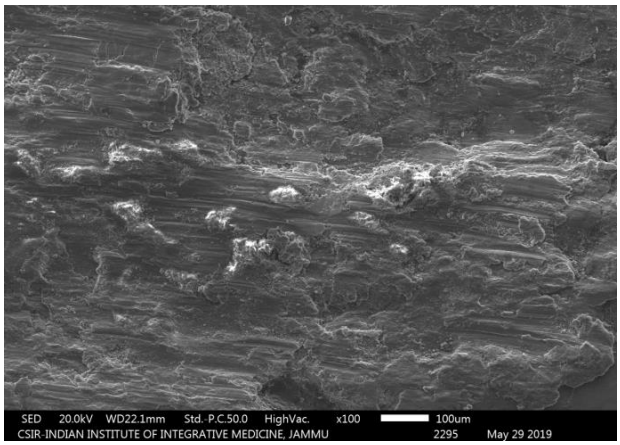

80 N load

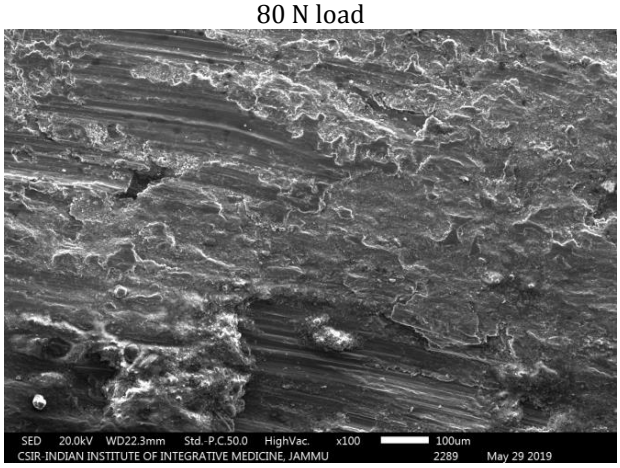

Sliding Distance (450 meters)

Fig. 16. SEM micrographs of Hybrid composition-6 (450 ˚C) wear scar (80 N; Sliding Distance).

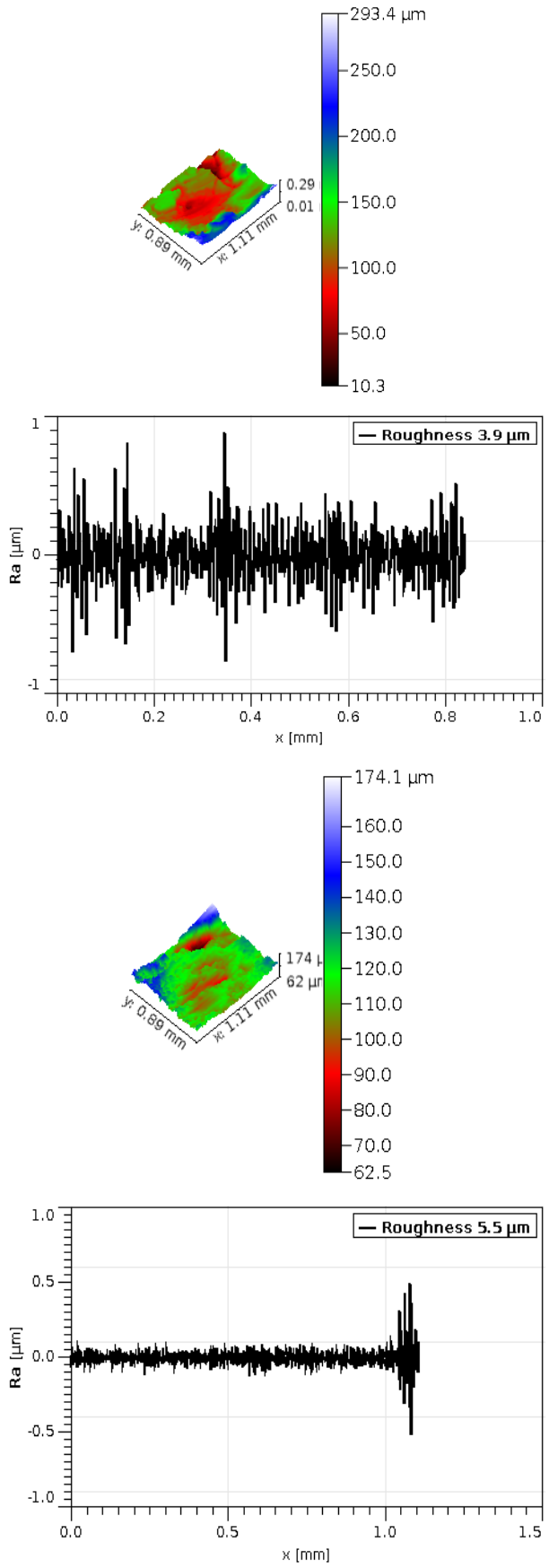

Fig. 17. 3-D Surface Profilometer micrographs of wear scar on Hybrid composition 6 (450 ˚C) (80 N; Sliding Distance 450 m).

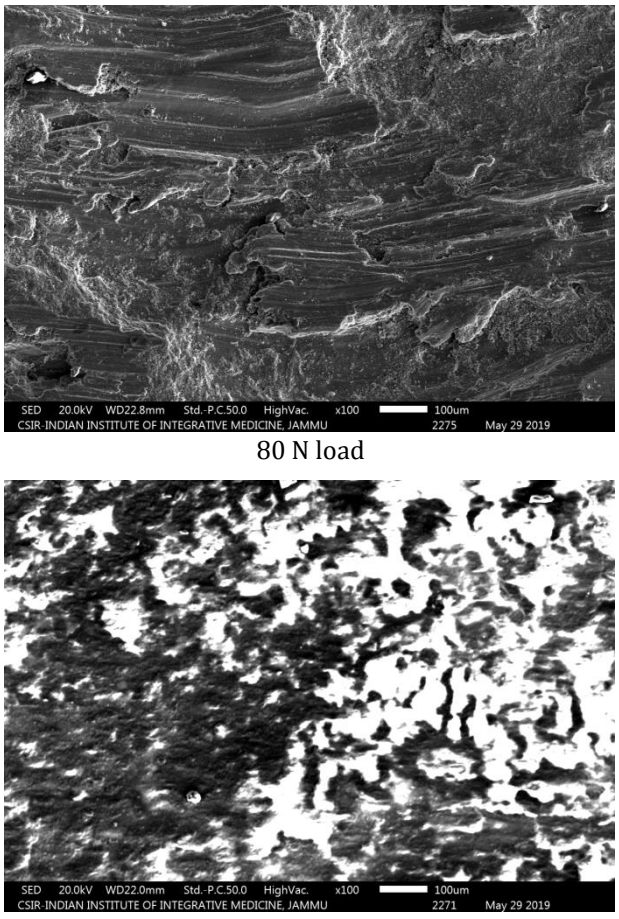

Fig. 18. SEM micrographs of Hybrid composition-6 (500 ˚C) wear scar (80 N; Sliding Distance).

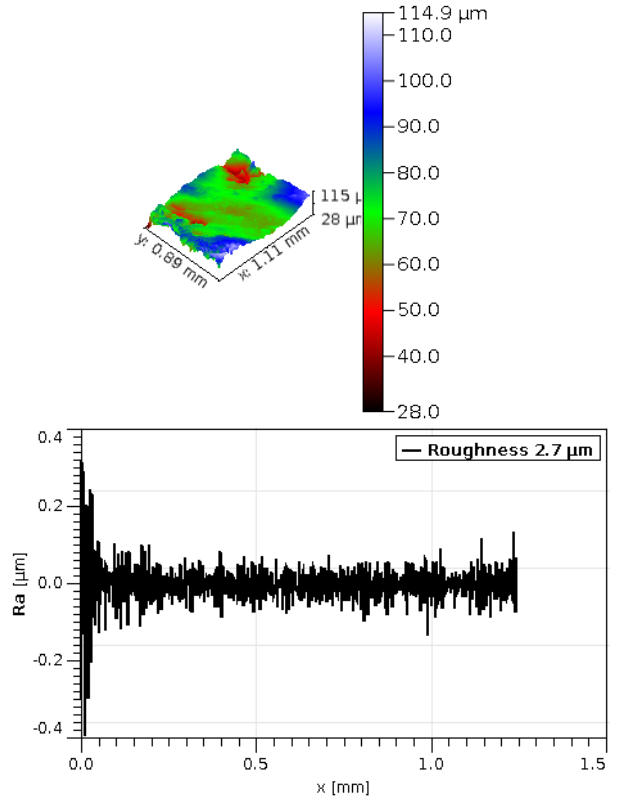

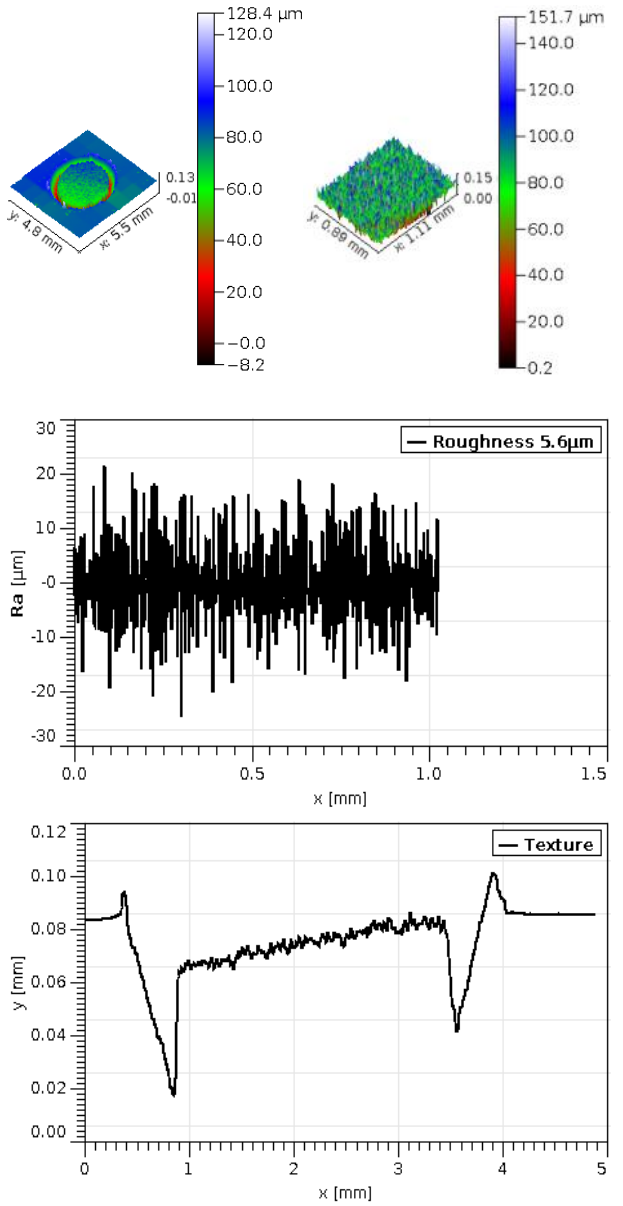

Fig. 19. 3-D Surface Profilometer micrographs of wear scar on Hybrid composition 6 (500 ˚C) (80 N; Sliding Distance 450 m).

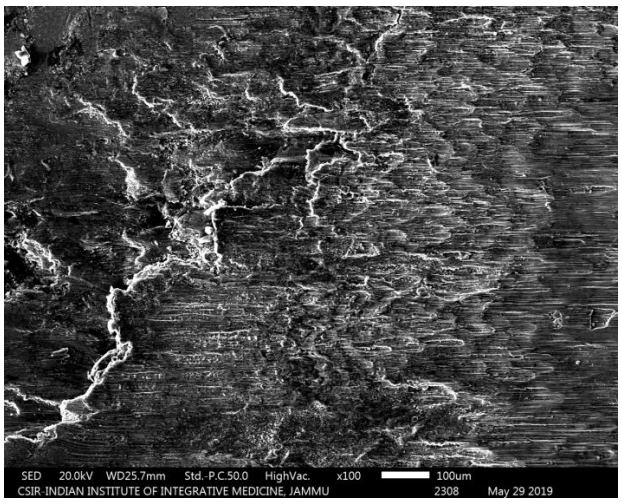

80 N load

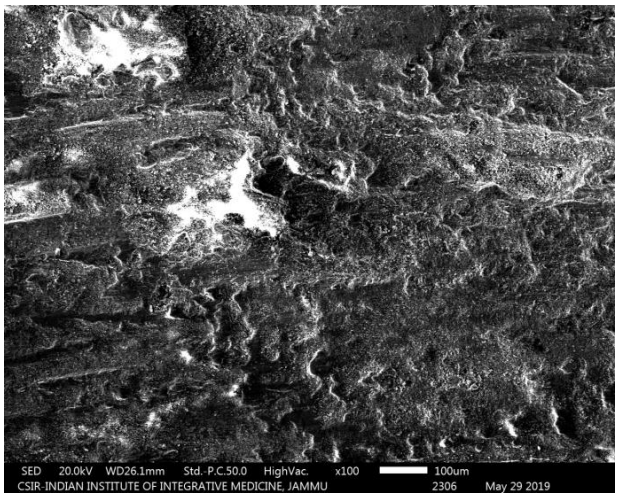

Sliding Distance (450 meters)

Fig. 20. SEM micrographs of Hybrid composition-6 (520 ˚C) wear scar (80 N; Sliding Distance).

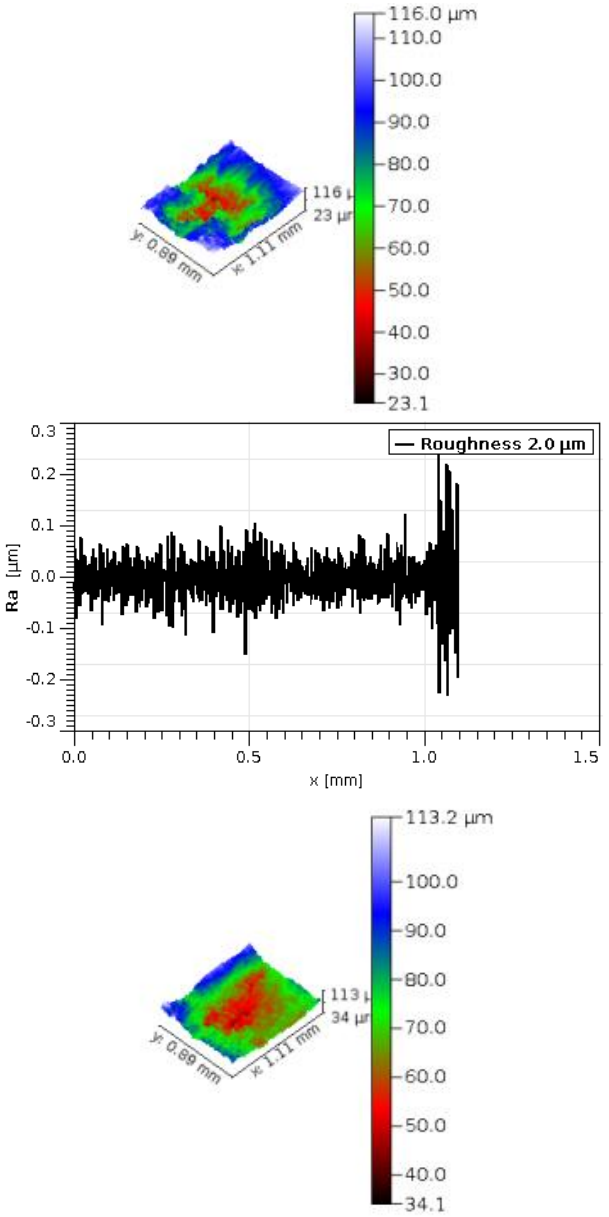

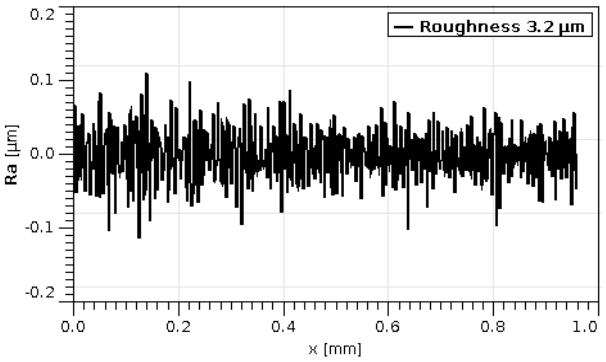

Fig. 21. 3-D Surface Profilometer micrographs of wear scar on Hybrid composition 6 (520 ˚C) (80 N; Sliding Distance 450 m).

3D surface profilometer studies were made on the wear scar of the hybrid composite testing under different loading conditions and variable sliding distance. 3D profilometer of wear tracks for HC5-450 shows (Ra) roughness of 3.0 µm, 3.0 µm, 3.4 µm, 3.9 µm at 10 N, 20 N, 50 N, 80 N load and 5.7 µm (Ra); for sliding distance 450 meters. For HC5-500, reduction in the Ra value was reported with roughness value 2.0 µm, 2.0 µm, 2.6 µm, 3.0 µm for 10 N, 20 N, 50 N, 80 N load respectively and 5.5 µm for 450 meters sliding distance. It was reported that a reduction in the surface roughness was reported for HC5-500 in comparison to HC5-450. It confirms that sintering temperature also plays a vital role in the surface wear texture and surface profile of the composite sample. Further, for HC6-450; HC6-500 & HC6-520 continuous reduction in the wear scar surface roughness was reported. HC6-520 reported a minimum surface roughness (Ra) 3.2 µm for 450 meter sliding distance and 2.0 µm (Ra) at 80 N load. Results indicate that graphene in the composite sample forms an oxide layer which smoothens the wear scar surface and minimizes the wear scar width and depth. This proves that the graphene oxide layer was stacked on the worm track during the tribo testing. The surface morphology indicate that the addition of the GNP considerably smoothen the surface by reducing the surface roughness [42]. It is attributed to the 2D GNP which provide easy shear due to weak vander wall force of the GNP particles. Moreover the GNP particles fill the deep grooves, scratches and cover this by tribofilms [43-44]. This also enhances the surface roughness of the composite sample. The results indicate that the surface roughness; texture as well as wavieness of the wear scar notably decreases with the addition od the GNP reinforcement.

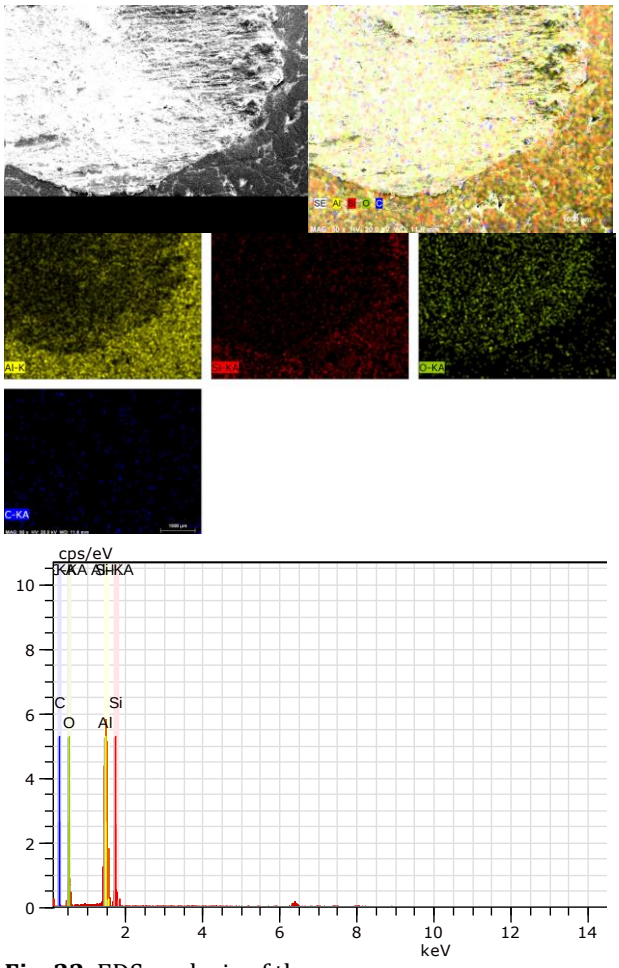

Fig. 22. EDS analysis of the wear scar.

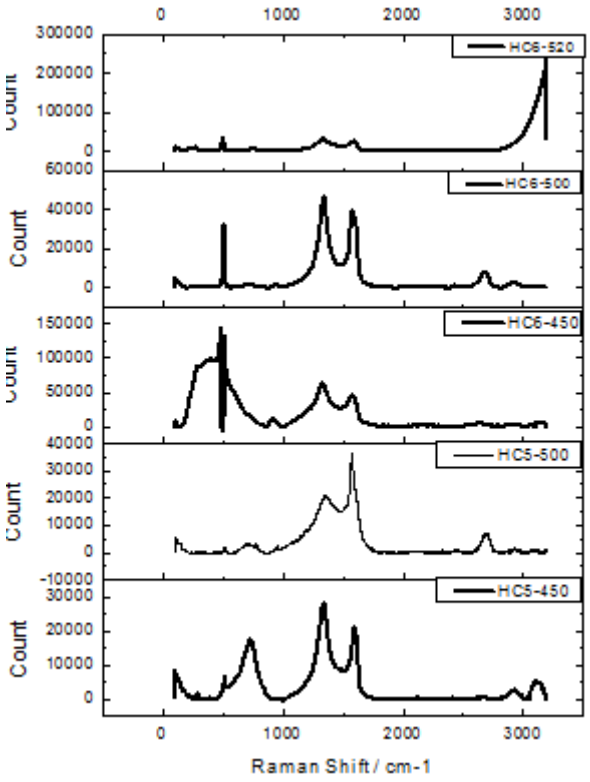

Fig. 23. Raman Shift analysis of the wear scar for different compositions samples.

Raman spectroscopy was used to study hybrid composite contain carbon phase particularly GNP after tribotesting. From the analysis presence of the graphene oxide protective layer on the rubbing, the contact surface was diagnosed. Raman morphology confirms that D, G, and 2D band on 1347 cm^{-1}, 1598 cm^{-1}, 2700 cm^{-1} which gives the evidence of protective layer formed on the wear scar.

4. CONCLUSION

In this current study, tribological experiment studies are conducted on novel hybrid self lubricating composites. On the basis of the results obtained from the experiments, it can be concluded that:

- Spark Plasma Sintering has a great impact on the tribological properties and make it possible to achieve near theoretical and dense composite samples. With increase in the sintering temperature the density of the fabricated sample increases.
- It was also reported that the alumina reinforcement effectively helps to increase the load-bearing capacity of the composite and GNP as secondary reinforcement provides a self-lubrication effect hence improve the friction and wear properties of the hybrid composite.
- GNP reinforcement in the matrix material acts as the solid lubricant and provides lubrication under dry sliding conditions. Therefore; it is reported that addition of the primary, as well as secondary reinforcement in the matrix material, improves the overall properties of the composite material.
- The wear mechanism of hybrid composite was characterized as adhesion, abrasion and plastic deformation.

The beneficial effects of SPS (fast sintering route), reinforcement concentration significantly reduce friction; wear and can be used for manufacturing various engine components. This study helps us to find new opportunities for eutectic Al-Si alloy for mechanical/ automotive applications.

Acknowledgments

I gratefully acknowledge all the researchers who have worked in the field of tribology. Without their significant contribution, this review literature would have been difficult to summarise. I would also want to acknowledge my institute and supervisor for their wholehearted support.

REFERENCES

[1] K.G. K.G. Budinski, M.K. Budinski: *Engineering materials: Properties ans Selection, 9th Edition*. Pearson, 2010.

[2] N.P. Suh, *The delamination theory of wear*, Wear, vol. 25, iss. 1, pp. 111-124, 1973, doi: 10.1016/0043-1648(73)90125-7

[3] H.C. Meng, K.C. Ludema, *Wear models and predictive equations: their form and content*, Wear, vol. 181-183, pp. 443-457, 1995, doi: 10.1016/0043-1648(95)90158-2

[4] J.M. Challen, P.L.B. Oxley, *An explanation of the different regimes of friction and wear using asperity deformation models*, Wear, vol. 53, iss. 2, pp. 229-243, 1979, doi: 10.1016/0043-1648(79)90080-2

[5] B. Bhushan, J.N. Israelachvili, U. Landman, *Nanotribology: friction, wear and lubrication at the atomic scale*, Nature, vol. 374, pp. 607-616, 1995, doi: 10.1038/374607a0

[6] D.H. Buckley: *Surface effects in adhesion, friction, wear, and lubrication*. Elsevier, 1981.

[7] K.C. Ludema, L. Ajayi: *Friction, wear, lubrication: a textbook in tribology*. CRC press, 2018.

[8] L. Merhari: *Hybrid nanocomposites for nanotechnology*. Springer, 2009, doi: 10.1007/978-0-387-30428-1

[9] C. Sanchez, B. Julián, P. Belleville, M. Popall, *Applications of hybrid organic–inorganic nanocomposites*, Journal of Materials Chemistry, vol. 15, iss. 35-36, pp. 3559-3592, 2005, doi: 10.1039/B509097K

[10] G. Kickelbick: *Hybrid materials: synthesis, characterization, and applications*. John Wiley & Sons, 2007.

[11] M.L.T. Guo, C.-Y.A. Tsao, *Tribological behavior of self-lubricating aluminium/SiC/graphite hybrid composites synthesized by the semi-solid powder-densification method*, Composites Science and Technology, vol. 60, iss. 1, pp. 65-74, 2000, doi: 10.1016/S0266-3538(99)00106-2

[12] A.D. Moghadam, B.F. Schultz, J.B. Ferguson, E. Omrani, P.K. Rohatgi, N. Gupta, *Functional metal matrix composites: self-lubricating, self-healing, and nanocomposites-an outlook*, vol. 66, iss. 6, pp. 872-881, 2014, doi: 10.1007/s11837-014-0948-5

[13] M. Omori, *Sintering, consolidation, reaction and crystal growth by the spark plasma system (SPS),* Materials Science and Engineering: A, vol. 287, iss. 2, pp. 183-188, 2000, doi: 10.1016/S0921-5093(00)00773-5

[14] A.Z. Munir, U. Anselmi-Tamburini, M. Ohyanagi, *The effect of electric field and pressure on the synthesis and consolidation of materials: A review of the spark plasma sintering method*, Journal of Materials Science, vol. 41, iss. 3, pp. 763-777, 2006, doi: 10.1007/s10853-006-6555-2

[15] O. Guillon, J. Gonzalez-Julian, B. Dargatz, T. Kessel, G. Schierning, J. Räthel, M. Herrmann, *Field-assisted sintering technology/spark plasma sintering: mechanisms, materials, and technology developments,* Advanced Engineering Materials, vol. 16, iss. 7, pp. 830-849, 2014, doi: 10.1002/adem.201300409

[16] Y.B. Liu, J.D. Hu, Z.Y. Cao, P.K. Rohatgi, *Wear resistance of laser processed Al–Si–graphite composites*, Wear, vol. 206, iss. 1-2, pp. 83-86, 1997, doi: 10.1016/S0043-1648(96)07496-0

[17] C.B. Lin, R.J. Chang, W.P. Weng, *A study on process and tribological behavior of Al alloy/Gr.(p) composite*, Wear, vol. 217, iss. 2, pp. 167-174, 1998, doi: 10.1016/S0043-1648(98)00192-6

[18] L. Krishnamurthy, B.K. Sridhara, D.A. Budan, *Comparative study on the machinability aspects of aluminium silicon carbide and aluminium graphite composites*, Materials and Manufacturing Processes, vol. 22, iss. 7-8, pp. 903-908, 2007, doi: 10.1080/10426910701451754

[19] S. Das, S.V. Prasad, T.R. Ramachandran, *Tribology of Al Si alloy-graphite composites: triboinduced graphite films and the role of silicon morphology*, Materials Science and Engineering: A, vol. 138, iss. 1, pp. 123-132, 1991, doi: 10.1016/0921-5093(91)90682-D

[20] M.L.T. Guo, C.Y. Tsao, *Tribological behavior of self-lubricating aluminium/SiC/graphite hybrid composites synthesized by the semi-solid powder-densification method*, Composites Science and Technology, vol. 60, no. 1, pp. 65-74, 2000, doi: 10.1016/S0266-3538(99)00106-2

[21] M.T. Guo, C.Y. Tsao, *Tribological behavior of aluminum/SiC/nickel-coated graphite hybrid composites,* Materials Science and Engineering: A, vol. 333, iss. 1-2, pp. 134-145, 2002, doi: 10.1016/S0921-5093(01)01817-2

[22] A.M. Hassan, A.S. Al-Bsharat, *Influence of burnishing process on surface roughness, hardness, and microstructure of some non-ferrous metals*, Wear, vol. 199, iss. 1, pp. 1-8, 1996, doi: 10.1016/0043-1648(95)06847-3

[23] A.R. Riahi, A.T. Alpas, *The role of tribo-layers on the sliding wear behavior of graphitic aluminum matrix composites*, Wear, vol. 251, iss. 1-12, pp. 1396-1407, 2001, doi: 10.1016/S0043-1648(01)00796-7

[24] S. Basavarajappa, G. Chandramohan, K. Mukund, M. Ashwin, M. Prabu, *Dry sliding wear behavior of Al 2219/SiCp-Gr hybrid metal matrix composites*, Journal of Materials Engineering and Performance, vol. 15, iss. 6, p. 668, 2006, doi: 10.1361/105994906X150803

[25] P.K. Rohatgi, R. Guo, J.K. Kim, S. Rao, T. Stephenson, T. Waner, Wear and friction of cast Al–SiC–Gr composites, in: Proceedings of materials solutions '97 on wear of engineering materials, 15–18 September, 1997, Indianapolis, Indiana, pp. 205-211.

[26] A. Ghazaly, B. Seif, H.G. Salem, *Mechanical and tribological properties of AA2124-grapheneself-lubricating nanocomposite*, Light Metals 2013, pp. 411-415, 2016, doi: 10.1007/978-3-319-65136-1_71

[27] F.P. Bowden, D. Tabor, *The area of contact between stationary and moving surfaces*, Proceedings of the Royal Society of London. Series A, Mathematical and Physical Sciences, vol. 169, iss. 938, pp. 391-413, 1939, doi: 10.1098/rspa.1939.0005

[28] G.J. Howell, A. Ball, *Dry sliding wear of particulate-reinforced aluminium alloys against automobile friction materials*, Wear, vol. 181-183, pp. 379-390, 1995, doi: 10.1016/0043-1648(95)90045-4

[29] M. Malaki, W. Xu, A. K. Kasar, P. L. Menezes, H. Dieringa, R. S. Varma, M. Gupta, *Advanced metal matrix nanocomposites*, Metals, vol. 9, no. 3, p. 330, 2019, doi: 10.3390/met9030330

[30] U. Anselmi-Tamburini, J. E. Garay, Z. Munir, A. Tacca, F. Maglia, G. Spinolo, *Spark plasma sintering and characterization of bulk nanostructured fully stabilized zirconia: Part I. Densification studies,* Journal of materials research, vol. 19, iss. 11, pp. 3255-3262, 2004, doi: 10.1557/JMR.2004.0423

[31] R. Ohser-Wiedemann, U. Martin, H.J. Seifert, A. Müller, *Densification behaviour of pure molybdenum powder by spark plasma sintering,* International Journal of Refractory Metals and Hard Materials, vol. 28, iss. 4, pp. 550-557, 2010, doi: 10.1016/j.ijrmhm.2010.03.003

[32] S. Hayun, S. Kalabukhov, V. Ezersky, M. P. Dariel, N. Frage, *Microstructural characterization of spark plasma sintered boron carbide ceramics,* Ceramics international, vol. 36, iss. 2, pp. 451-457, 2010, doi: 10.1016/j.ceramint.2012.05.003

[33] I. Aliyu, N. Saheb, S. Hassan, N. Al-Aqeeli, *Microstructure and properties of spark plasma sintered aluminum containing 1 wt.% SiC nanoparticles*, Metals, vol. 5, no. 1, pp. 70-83, 2015, doi: 10.3390/met5010070

[34] M.K.A. Ali, H. Xianjun, *M50 Matrix Sintered with Nanoscale Solid Lubricants Shows Enhanced Self-lubricating Properties Under Dry Sliding at Different Temperatures,* Tribology Letters, vol. 67, pp. 71, 2019, doi: 10.1007/s11249-019-1183-6

[35] I.K. Aliyu, *Effect of process parameters on microstructure and properties of spark plasma sintered Al-SiC nanocomposites,* Doctoral dissertation, King Fahd University of Petroleum and Minerals Saudi Arabia, 2013.

[36] N. Al-Aqeeli, K. Abdullahi, A.S. Hakeem, C. Suryanarayana, T. Laoui, S. Nouari, *Synthesis, characterisation and mechanical properties of SiC reinforced Al based nanocomposites processed by MA and SPS,* Powder Metallurgy, vol. 56, iss. 2, pp. 149-157, 2013, doi: 10.1179/1743290112Y.0000000029

[37] F.A. Essa, Q. Zhang, X. Huang, M.K.A. Ali, A. Elagouz, M.A. Abdelkareem, *Effects of ZnO and MoS 2 solid lubricants on mechanical and tribological properties of M50-steel-based composites at high temperatures: experimental and simulation study*, Tribology Letters, vol. 65, pp. 97, 2017, doi: 10.1007/s11249-017-0880-2

[38] M.K.A. Ali, P. Fuming, H.A. Younus, M.A. Abdelkareem, F.A. Essa, A. Elagouz, H. Xianjun, *Fuel economy in gasoline engines using Al2O3/TiO2 nanomaterials as nanolubricant additives,* Applied Energy, vol. 211, pp. 461-478, 2018, doi: 10.1016/j.apenergy.2017.11.013

[39] M.K.A. Ali, H. Xianjun, L. Mai, C. Qingping, R.F. Turkson, C. Bicheng, *Improving the tribological characteristics of piston ring assembly in automotive engines using Al_2O_3 and TiO_2 nanomaterials as nano-lubricant additives,* Tribology International, vol. 103, pp. 540-554, 2016, doi: 10.1016/j.triboint.2016.08.011

[40] M.K.A. Ali, H. Xianjun, F.A. Essa, M.A. Abdelkareem, A. Elagouz, S. W. Sharshir, *Friction and wear reduction mechanisms of the reciprocating contact interfaces using nanolubricant under different loads and speeds,* Journal of Tribology, vol. 140, iss. 5, p. 051606, 2018, doi: 10.1115/1.4039720

[41] F.A. Essa, Q. Zhang, X. Huang, A.M.M. Ibrahim, M.K.A. Ali, M.A. Abdelkareem, A. Elagouz, *Improved friction and wear of M50 steel composites incorporated with ZnO as a solid lubricant with different concentrations under different loads,* Journal of Materials Engineering and Performance, vol. 26, iss. 10, pp. 4855-4866, 2017, doi: 10.1007/s11665-017-2958-2

[42] P. Kumar, M.F. Wani, *Effect of load on the tribological properties of hypereutectic Al–Si alloy under boundary lubrication conditions,* Materials Research Express, vol. 4, iss. 11, pp. 116519, 2017, doi: 10.1088/2053-1591/aa98e5

[43] P. Kumar, M.F. Wani, *Tribological Characterization of Hypereutectic Al–25Si Alloy Under Dry and Lubricated Sliding Conditions,* Journal of Tribology, vol. 140, iss. 1, pp. 011603, 2018, doi: 10.1115/1.4036918

[44] P. Kumar, M.F. Wani, *Tribological characterisation of graphene oxide as lubricant additive on hypereutectic Al-25Si/steel tribopair,* Tribology Transactions, vol. 61, iss. 2, pp. 335-346, 2018, doi: 10.1080/10402004.2017.1322735

[45] T.H. Kosel, *ASM hand book, Volume 18: Friction, lubrication, and wear technology,* ASM International Handbook Committee, 1992.

[46] E. Rabinowicz, *The determination of the compatibility of metals through static friction tests,* ASLE Transactions, vol. 14, iss. 3, pp. 198-205, 1971, doi: 10.1080/05698197108983243